Design and fabrication of an insect-scale flying robot for control autonomy

Kevin Y. Ma, Pakpong Chirarattananon, Robert J. Wood

***Abstract*— Without sufficient payload capacity to carry necessary electronic components, flying robots at the scale of insects cannot fly autonomously. Using a simple scaling heuristic to define a few salient vehicle parameters, we develop a vehicle design that possesses the requisite payload capacity for the full suite of required components for control autonomy. We construct the vehicle using state-of-the-art methods, producing a 265 mg vehicle with a 115 mg payload capacity and demonstrate controlled stationary hovering of the fully-loaded vehicle. The payload-capable vehicle demonstrated here establishes a vehicle design and fabrication framework that will closely reflect that of an eventual, fully integrated robotic system.**

I. Introduction

The number of robotic air vehicles that utilize flapping wing flight has rapidly grown in the last decade. Notable examples include the Aerovironment Nanohummingbird [1] and the DelFly [2]. These two examples in particular have achieved controlled flight, either teleoperated or autonomous. At the scale of small birds, these robotic vehicles have sufficient payload capacity to carry consumer-grade RC components and control electronics.

Robotic flying vehicles at the scale of insects have also been in development for many years, but only in recent years have new innovations in design and manufacturing enabled these tiny robotic systems to be reliably constructed and proven flightworthy. The key early prototype in [3] demonstrated sufficient thrust forces to fly but couldn't generate control torques to maneuver. Advances in micromanufacturing centered around 2D laminate construction of dynamic, small-scale mechanisms [4] enabled the construction of more sophisticated mechanical designs where fabrication precision was crucial to their operation.

Based on that early prototype, a vehicle design, deemed the "split actuator microrobotic bee," demonstrated the ability to generate both sufficient thrust to lift its own weight and body torques for flight stabilization [5]. With the addition of a closed loop flight controller, the microrobotic bee successfully demonstrated controlled hovering and basic flight maneuvers [6]. The vehicle design has become a crucial research platform for developing flight controllers [7] and sensor suites for insect-scale, flapping-wing micro air vehicles. Sensors that have been implemented on the flying robot include an ocelli (light sensing array), gyroscope, and magnetometer [8], [9], [10].

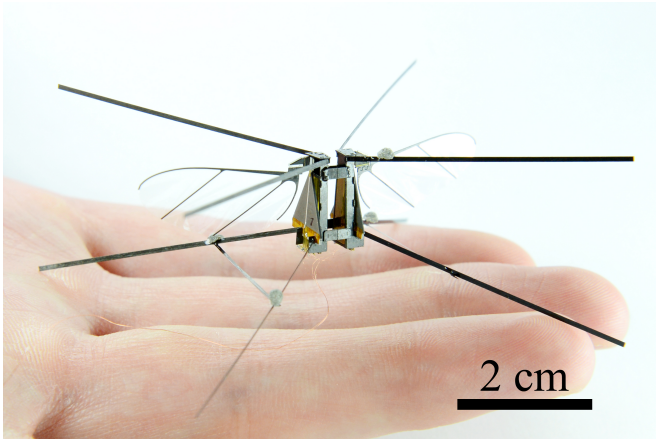

Fig. 1. The prototype robotic flying insect shown here has a wingspan of 5.5 cm and a mass of 380 mg when fully loaded. It has spars extending off the airframe that act as a roll cage to protect the wings from crash damage. Motion tracking markers for control are also attached to these spars.

However, the microrobotic bee as presented in [6] has a limited payload capacity and cannot simultaneously carry the requisite sensors, control and power electronics, and a power source for power and control autonomy. Thus far, the operation of the robotic vehicle has required a wire tether for power and control signal input. Flight controller development has relied on offboard motion capture for sensing vehicle dynamics. In addition, when the vehicle is loaded near its payload limits, less thrust force can be allocated for control purposes, rendering the vehicle performance extremely sensitive to onboard mass distribution. Research pace is significantly impeded by these limitations.

To improve the development pace of flight control theory and onboard sensors and electronics as well as to provide a more robust research platform, we are developing a robotic vehicle with more payload capacity and flight control margins than the split actuator microrobotic bee. The scaling laws of flapping-wing micro air vehicles have been explored in theory [11], [12], and these system-level analyses have provided key relationships between the critical vehicle design parameters. Relying on best-effort modeling of subcomponents, these studies seek to optimize the vehicle designs for flight endurance, among other performance metrics.

In this paper, we are not optimizing for a particular vehicle performance metric. Instead, we are focused on guiding the vehicle design and the manufacturing framework for this specific vehicle size range. Ideally, the chosen design can accomodate design changes from future optimizations of

This work was partially supported by the National Science Foundation (award number CCF-0926148) for Kevin Ma and the Wyss Institute for Biologically Inspired Engineering. Any opinions, findings, and conclusions or recommendations expressed in this material are those of the authors and do not necessarily reflect the views of the National Science Foundation.
The authors are with the School of Engineering and Applied Sciences and the Wyss Institute for Biologically Inspired Engineering, Harvard University, Cambridge, MA 02138. kevinma@seas.harvard.edu

Preprint submitted to 2015 IEEE/RSJ International Conference on Intelligent Robots and Systems. Received March 4, 2015.

performance metrics.

We are interested in a design that is extensible for scaling and imminent electronics integration. The design should accomodate multiple actuator sizes without significant changes to the structural design. Certain electronic sensors may have preferential placement in the vehicle hull; an adaptable scaffold for the integration of electronics would ensure the design is future-proof.

Additional impediments for research pace include the difficult construction process and limited mechanical lifetime of the current vehicle design. In particular, the actuators, wings, and flexure hinges are susceptible to mechanical fatigue and permanent damage from flight crashes. Research efforts to improve mechanical lifetime and construction efficiency have been fruitful. The fatigue characteristics of the flexure hinges that constitute the transmission mechanism have been explored [13]. Actuator fabrication processes, mechanical performance, and lifetime have improved [14]. The pop-up manufacturing methodology presented in [4] provides a path for efficient, precise construction of robots. These developments form a critical tool set for us as we are interested in a vehicle design that is straightforward in its construction and can be repeatably produced en masse while slowing the rate at which vehicles mechanically break down.

In this paper, we present a scaling heuristic for the vehicle design and use it to identify scaling goals for the critical components in the robotic vehicle. We apply the latest fabrication methods for the various vehicle components and also present additional refinements to existing fabrication methods. Design decisions are made to best support research and development pace in terms of ease of vehicle construction en masse and mechanical robustness of the vehicle. We constructed a 265 mg flying vehicle, based on the vehicle design of the split actuator microrobotic bee from [5] but with 3 times the payload capacity, and demonstrated closed-loop, controlled hovering flight with a 115 mg dummy payload onboard.

II. System design

A. Design goals

The robotic vehicle presented in this paper is based on the design of the "split actuator bee" in [5]. The design has two flapping wings, each wing independently driven with a separate piezoelectric linear actuator. Two separately driven wings enable the vehicle to generate body torques, which is crucial to stabilize and maneuver in flight. The method of driving the wings for torque generation is described in [5] and [6]. Much of the split actuator bee design was based off of a legacy vehicle design [3] which first demonstrated an insect-scale, piezoelectric-driven flapping wing mechanism with enough thrust force to take off. From the analyses performed in [18], we know that a flapping wing mechanism driven by piezoelectric linear actuators can be approximated as a harmonic oscillator. Thus, we can identify a distinct natural frequency at which wing stroke amplitudes, and therefore mechanical energy transfer, is greatest.

The work presented here is concerned with developing a mechanical design and manufacturing framework on which to further optimize the vehicle parameters. In addition, we want a flight-capable vehicle with more payload in order to support research efforts for onboard electronics integration. As such, we only need to roughly calculate the component dimensions for a scaled up vehicle capable of carrying more payload. This larger vehicle will more closely match the scale and design of an eventual, fully power-autonomous vehicle; thus the design and manufacturing framework developed would not need to change drastically. Here, we present our heuristic for scaling up the vehicle design.

The full system-level optimization of flapping wing air vehicles is a complex, high-dimensional problem with significant interdependence between various design parameters. For example, we desire more payload capacity on our vehicle and thus more thrust. Intuitively, to perform more work against the air and generate more thrust force, the vehicle design needs either larger wings or higher flapping frequency. Additionally, wing pitch rotation—a key element of the wing kinematics for both insects and robots [3], [19]—relies on the interplay of aerodynamic and inertial forces acting on an elastically deforming wing hinge to deflect and pitch the wing. When the wing length, inertia, or flapping frequency change, the wing pitching dynamics also change as a secondary effect and alter the wing's lift and drag coefficients. This will affect the system dynamics which in turn alter the flapping kinematics. The scaling laws for flapping-wing aerodynamics [11] and system dynamics, in addition to power efficiency considerations [16], need to be reconciled simultaneously to identify the design space for a high-performance air vehicle.

To expedite the scaling analysis, we hold constant all key design parameters except the wing length and the flapping frequency. To preserve the wing kinematics of the split actuator bee design, we set the transmission ratio to $T = 3.28$ rad/mm and the actuator free peak-to-peak displacement amplitude to $\delta = 0.85$ mm. For the wing shape, we use the wing morphology from the experiments of [20], with a second moment of area, $\hat{r_2}$, of 0.55 and an aspect ratio of 3. This wing shape was found to be an improvement in lift-to-drag ratio over that of the split actuator bee. The wing is now parameterized by a single wing length scaling factor, which will scale the wing planform dimensions proportionally.

To determine the wing length and flapping frequency, we apply two constraints in the system modeling. First, the vehicle must generate a required thrust force. Second, the vehicle's flapping-wing system should be operating at its natural frequency.

To determine the required thrust force, we must estimate the payload of the target vehicle. Table I lists the minimum known set of electronic components needed for autonomous flight control, as of the writing of this paper, and the mass of each component. Noticeably missing from Table I is an onboard battery for powering the robotic vehicle. For the sake of near-term research progress, our working goal for this paper is control autonomy—not power autonomy—and assume that electrical power will be fed to the robot through

Preprint submitted to 2015 IEEE/RSJ International Conference
on Intelligent Robots and Systems. Received March 4, 2015.

TABLE I

ELECTRONIC COMPONENTS NECESSARY FOR CONTROL AUTONOMY

Component	Mass (mg)	Additional physical requirements
"Brain" chip (System-on-Chip microprocessor) [15]	10	
Power electronics [16]	40	Place close to the vehicle base
Inertial measurement unit (IMU) (gyroscope+accelerometer) (Invensense MPU6500)	25	Place close as possible to vehicle center of mass
Optic flow sensor [17]	15	Place downward facing with unobstructed view
Flexible Kapton PCB and electronic integration overhead	10	
Total	100	

TABLE II

DESIGN PARAMETERS FROM THE SPLIT ACTUATOR BEE IN [5]. DESIGN GOALS AND RESULTS FOR THE SCALED UP ROBOTIC BEE

Vehicle parameter	Units	Split actuator bee	Scaled goals	Scale factor	Scaled results
Flapping frequency	Hz	100	60–85	0.6–0.85	70
Wing length	mm	15	26	1.7	26
Measured maximum thrust force	mg	140	414		450
Total actuator mass	mg	50	150	3	196
Total unloaded robot mass	mg	80	240	3	265
Measured payload capacity (includes mass of roll cage)	mg	35	105	3	115
Total loaded robot mass	mg	115	345	3	380
Actuator mass fraction		0.625	0.625	1	0.74
Mechanism and structure mass fraction		0.375	0.375	1	0.26
Thrust-to-weight ratio		1.75	1.725		1.70

a wire tether—similar to the flights first demonstrated in [6]. A more directed effort to reduce battery mass and increase battery energy density is needed prior to adding its mass contribution to the robot's payload.

In addition to the electronics' static payload contribution, we look toward the component mass fractions of the split actuator bee for further design direction. Relevant numbers for this discussion from the previous design are listed in Table II. We hypothesize that a larger scale vehicle would have similar actuator mass fractions, extrapolating from observations on flying insects that found muscle mass fraction to be the best indicator of thrust-to-weight ratio [21]. The split actuator bee has a payload capacity in controlled flight of about 35 mg [9], on top of a 80 mg unloaded body mass. Based on the 100 mg known total payload needed for control autonomy from Table I, we choose a vehicle with at least 3 times the payload capacity of the split actuator bee in order to carry it, or 105 mg. This would entail a robot with body mass of 240 mg, for a total loaded robot mass of 345 mg. Of the 240 mg body mass, 5/8 would be actuator mass, or 150 mg, and 3/8 would be mechanism and structure mass, or 90 mg.

Additionally, the split actuator bee has a thrust-to-weight ratio of 1.75 when unloaded and a thrust-to-weight ratio of 1.2 when loaded. The 20% thrust force overhead beyond the weight of a fully loaded robot is needed in order to generate flight control torques and accelerations. The piezoelectric bimorph cantilever actuators practically operate within voltage bounds from 0-300V, constrained by the ceramic material's strain limits. Within those bounds, a sinusoidal driving signal of varying amplitude and offset can operate. Signal amplitude modulates wing stroke amplitude and thus thrust magnitude. Signal offset modulates the mean wing stroke angle and is used to generate pitch torque in the vehicle by moving the thrust vector fore-aft relative to the vehicle center of mass. If the thrust needed to lift the vehicle is very large, signal amplitudes will increase until maxing out the 300V range. Near this operating point, achievable signal offsets become very limited, which will limit the pitch torque generation ability and consequently the flight stability and control authority of the vehicle. Thus, the required maximum thrust force from the vehicle is $1.2 \times 345 = 414$ mg, which is about 3 times the maximum measured thrust force from the split actuator bee. The design goals for the scaled vehicle are listed in Table II.

B. Scaling heuristic

Aerodynamic forces stemming from flapping wings can be estimated with the blade element method, as described in [12]. The resulting scaling relationship between aerodynamic force F_L, wing length R, and flapping frequency f is:

$$F_L \propto R^4 \cdot f^2 \tag{1}$$

Approximating the system as a harmonic oscillator provides an expression, shown in Eq.2, for the system's natural frequency ω_n, which relates the wing design, actuator design, and operating frequency. This relationship assumes that the actuators are the primary contributors of system stiffness k_{act} and that the wings are the primary contributors of system inertia I_{wing}. This was shown to be a valid assumption in [18].

$$\omega_n = \sqrt{\frac{k_{act}}{I_{wing}}} \tag{2}$$

The required blocked force from the actuators F_b to lift a flapping wing vehicle with mass W was approximated by Eq.14 of [12], reproduced here:

$$F_b = W \frac{\widetilde{C_D}}{\frac{1}{2}\widetilde{C_L}} \cdot \hat{Tr_{cp}} R \tag{3}$$

Preprint submitted to 2015 IEEE/RSJ International Conference on Intelligent Robots and Systems. Received March 4, 2015.

This equation assumes the vehicle is in stationary hover, and its mass is exactly offset by the lift force it generates. The actuator relates to the vehicle mass as drag force, calculated using the lift-to-drag ratio $\widetilde{C_L}/\widetilde{C_D}$. Additional terms are the transmission ratio T and non-dimensional wing center of pressure radius $\hat{r_{cp}}$; these two quantities are fixed in this analysis. Actuator stiffness k_{act} is approximated as the ratio of blocked force F_b to free displacement. Assuming free displacement is constant, the scaling relationship between actuator stiffness, vehicle mass, and wing length is:

$$k_{act} \propto W \cdot R \tag{4}$$

Wing inertia is related to the wing morphology. Previous studies of system dynamics have modeled the wings as a simple beam of constant cross-sectional area in order to generate a general expression for wing inertia [12], [18]. Here, because we have fixed the wing shape, we can use CAD modeling to empirically determine the wing inertia as a function of wing length for this particular wing shape. We determined the scaling law through manual fitting of a power function and found it to be:

$$I_{wing} \propto R^{3.7} \tag{5}$$

Consequently, combining Eq.4 and Eq.5 with Eq.2 results in the following scaling relationship for natural frequency, vehicle mass, and wing length:

$$\omega_n \propto W^{0.5} \cdot R^{-2.7} \tag{6}$$

To meet both of our design constraints, we equate flapping frequency f with natural frequency ω_n and vehicle mass W with required thrust force F_L. This is justified because the thrust and drag forces scale similarly and, when mapped through the transmission ratio T to the actuator, are proportional to the actuator blocked force F_b.

Figure 2 shows Eq.1 and Eq.6 with $F_L = W = 3$ times the magnitude of the split actuator bee, plotted over the flapping frequency scaling factor vs. wing length scaling factor space. Intuitively, a vehicle with 3 times more thrust force will have larger wings flapping at a lower frequency which is limited by finite wing inertia. Based on the plot of system dynamics from Eq.6, to ensure a flapping frequency scaling of less than 1, the wing length must be at least 1.3 times longer. Aerodynamic scaling from Eq.1 dictates a wing length 1.5 times longer to ensure a flapping frequency scaling of less than 1. We can interpret these curves as an upper and lower bound on the natural frequency, to determine the target flapping frequency for a given wing length.

Based on previous fabrication experience and intuition, we believe it would be difficult to increase wing length by more than 50% without a decrease in the natural frequency less than 10%. Thus, we choose a wing length scaling of 1.7 so that our upper bound on the target frequency is managably lower, at a decrease of 15%. Our scaling target for the larger vehicle design is a 1.7 times longer wing length and 0.6–0.85 times greater flapping frequency, scaled relative to the split actuator bee vehicle design of [5]. Table II lists the target design parameters for the scaled up robotic bee.

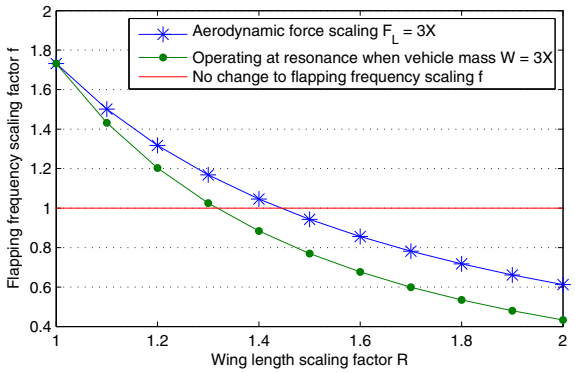

Fig. 2. Scaling relationships between flapping frequency and wing length, derived from wing kinematics to ensure 3 times the thrust force output (Eq.1) and system dynamics to ensure efficient operation at resonance (Eq.6).

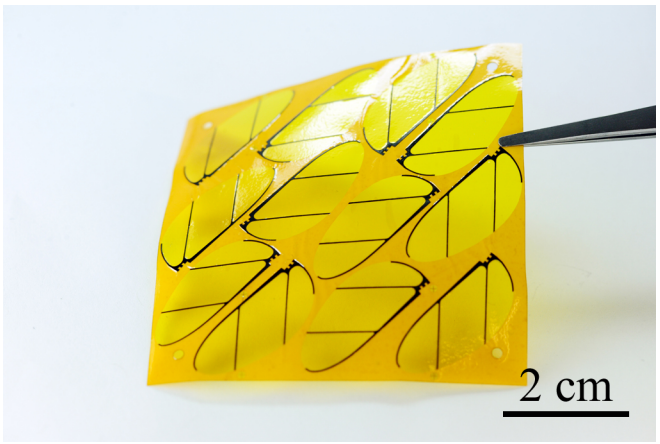

Fig. 3. Wings are efficiently made in batches, by laminating monolithically-cut carbon fiber composite frames to thin polyester film. A precision laser release cut will extract the individual wings from the bulk laminate.

III. Fabrication Framework

In determining our fabrication methods, we are reconciling the need for high-performance components with the efficiency of their production. A fabrication method that achieves both goals tends to be more difficult and time-consuming to develop. Automated methods like pop-up manufacturing [4] increase yield rates but are difficult to design and implement, slowing down prototyping and iteration pace. Manual assembly methods are faster to implement and flexible to design changes but are tedious, imprecise, and difficult to scale for large numbers. For research and development purposes, we are interested in producing on the order of 10 vehicles. Based on our prior fabrication experience, we have identified a particular balance of manual and automated methods for subcomponents to achieve these numbers efficiently.

A. Wings

The wing shape is fixed as described in Section 2A. A number of requirements influence the wing fabrication development. They should be very low mass to limit inertia. They should also be strong enough to resist the resulting

Preprint submitted to 2015 IEEE/RSJ International Conference on Intelligent Robots and Systems. Received March 4, 2015.

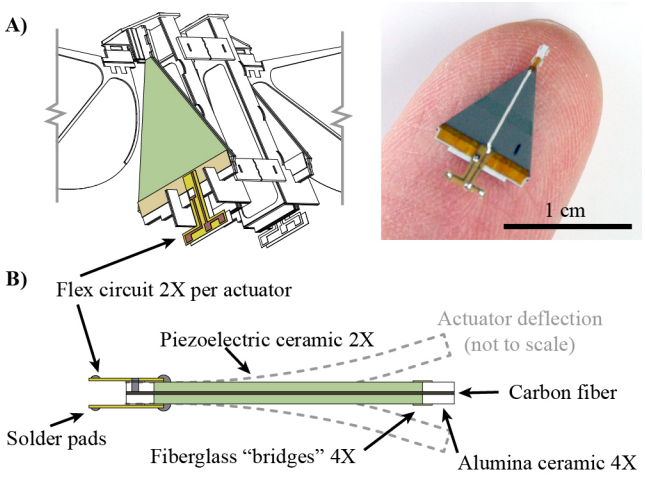

Fig. 4. A) Wiring of the vehicle's piezoelectric bimorph actuators is performed manually. Discrete flex circuit elements are implemented on the actuators to extend the electrical contacts below the vehicle and facilitate manual electrical interfacing. B) The actuators are layered composite beams of piezoelectric ceramic (PZT-5H), alumina ceramic for the base and tip, and carbon fiber for the central elastic layer [14]. Fiberglass "bridges" reinforce the four ceramic material interfaces. Flex circuits with accessible solder pads are attached to electrically interface with the actuators. Actuator not shown to scale.

drag forces from flapping without much deformation and to survive rough crash landings. Lastly, the fabrication process should be reliable, repeatable, and able to produce multiple wings efficiently.

The previous method of wing production, used in [5], adhered a thin, 1.5 μm polyester film onto a carbon fiber frame cut from 80 μm precured carbon fiber composite sheets. The simplicity of monolithically cutting the entire wing frame out of uniformly thick material enabled efficient, reliable production of wings. Wings are fabricated separately and manually assembled to the transmissions in order to facilitate broken wing replacement.

Because the new wings are larger and will carry more payload, they will experience greater aerodynamic loading. As a simple approximation, we are using a wing that is 1.7 times longer to generate 3 times more lift and drag force. This translates to 2.1 times the normal force on the wing, assuming a wing pitch angle of 45° where lift and drag forces are approximately the same. This will increase the bending moment on the wing by 3.6 times. We iterated on a few methods for producing lightweight, strong wings and eventually settled on a small modification to the previous fabrication method that retained the method's efficiency and reliability while increasing the wing's bending stiffness. The carbon fiber composite sheets are now made 50% thicker at 120 μm which, assuming consistent material properties, increases the bending stiffness by 3.4 times and the approaches the estimated increase in wing loads. To support prototype testing and prevent wing damage, we add a roll cage consisting of thin carbon fiber spars to prevent the wings from hitting the ground, as seen in Figure 1. Figure 3 shows a complete laminated palette of wings prior to release from the bulk laminate.

B. Actuators

The piezoelectric ceramic bimorph actuators used in the vehicle are based on the design from [22]. Improvements to the manufacturing and performance of these actuators are presented in [14] and represent the state-of-the-art. A few additions were made to the actuators used in this vehicle design. We use non-conductive fiber glass "bridges" instead of conductive carbon fiber bridges to decrease the chance that damage to the electrically-insulating parylene coating will cause an electrical short. We also add discrete flex circuit components to the actuators, so that the electrical interface to them can extend below the base of the vehicle and make the electrical wiring task easier (see Figure 4).

We use the actuator model from [22] to determine dimensions for the larger actuators. Because our improved manufacturing processes have allow for increased voltage operation, we use higher fields (350V bias voltage) in our calculations while maintaining the same actuator output displacement from the split actuator bee in order to preserve its wing kinematics. This results in a shorter actuator length of 8.332 mm versus the 9 mm length from the split actuator bee. The increased length of the wings and the increased wing loading results in a 5.1 times larger blocked force requirement for the actuators. To compensate for the larger force requirement, we must increase the width of the actuators according to the theory presented in [22], which describes blocked force as proportional to the nominal width of the actuator. The new nominal actuator width is 8.606 mm, compared to 1.125 mm from the split actuator bee.

C. Transmission

The transmission is a four-bar linkage that converts the motion of the actuator tip to flapping wing motion. Kinematically, this requires a conversion of the rotational tip motion of the bimorph actuators to the rotational motion of the flapping wings. This was realized with a spherical four-bar mechanism in the split actuator bee design [5]. However, the spherical four-bar nature of the transmission required a delicate manual folding and assembly procedure that was vulnerable to human error. It is also not clear that a spherical four-bar was needed, given the very limited bimorph actuator tip rotation; the total rotational deflection of the actuator tips is <5° and the lengthwise tip displacement is negligible (<7 μm). Thus, motivated by the difficulty of the manual folding procedure, we rely instead on the pop-up manufacturing method and produced the four-bar mechanism with a five rigid-layer laminate that outputs a fully assembled transmission with no further manual steps, identical to the transmission used in pop-up bee design [4]. Figure 5B further illustrates the operation and construction of the transmission. We have empirically found that this planar four-bar mechanism can perform its motion-conversion role without noticeably affecting the system dynamics. The off-axis compliance of the flexure hinges in the mechanism is able to absorb the twist angle from the slight rotations of the actuator tips. As described in Section 2A, the transmission ratio remains the same as that of the split actuator bee.

Preprint submitted to 2015 IEEE/RSJ International Conference
on Intelligent Robots and Systems. Received March 4, 2015.

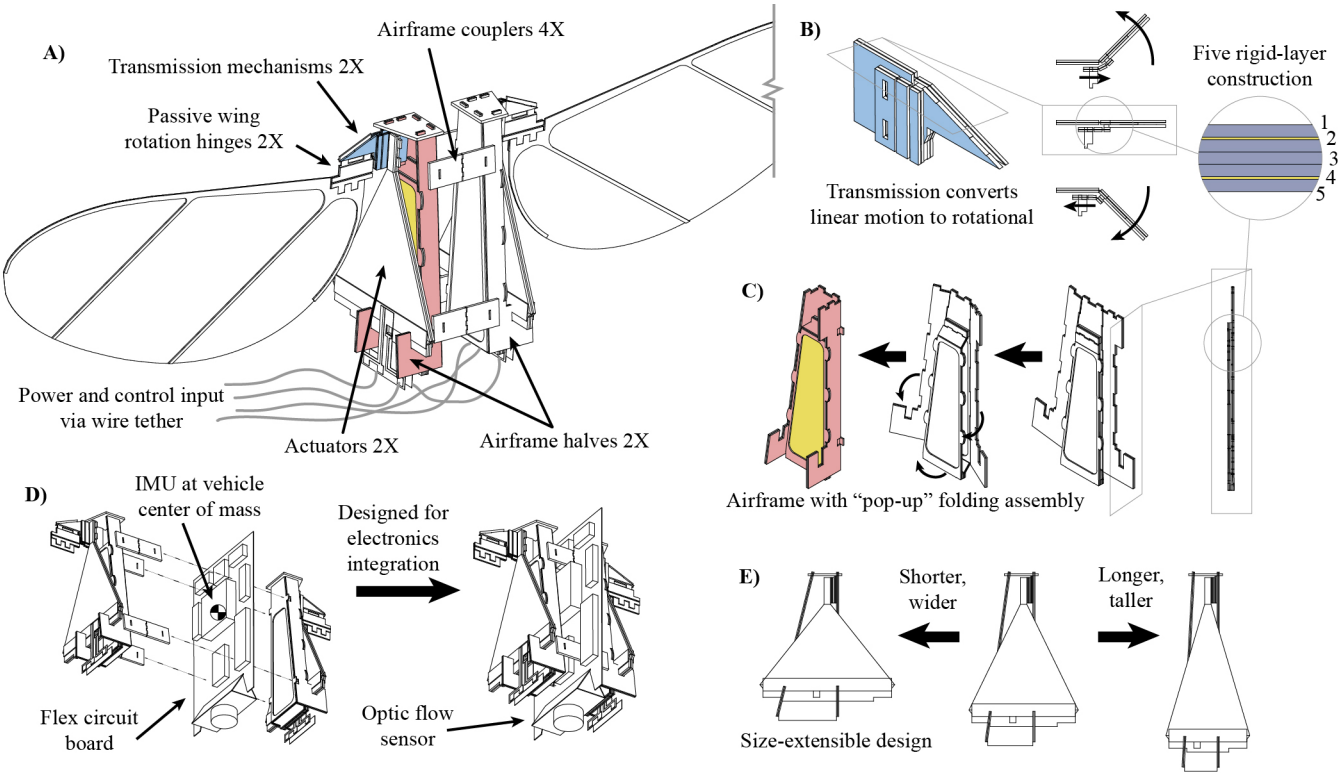

Fig. 5. Construction details for the robotic flying insect. A) Assembly of components that make up the vehicle. B) The transmission converts the nominally linear actuator tip motion to a rotational flapping motion. It is constructed with laminated layers of rigid carbon fiber composite and flexible polyimide film and consists of five rigid layers. C) The airframe is a rectangular thin-walled tube structure, designed for efficient bending and torsional resistance. Similarly with the transmission, it consists of five rigid layers of carbon fiber composite and can be fabricated simultaneously with the transmission. The design is a pop-up structure for ease of assembly. Polyimide film membrane (colored yellow) stretches across the broad faces—a semi-monocoque airframe. D) Extensibility for electronic integration. The electronic components will populate a flex circuit board that resides in the central plane of the vehicle, establishing a straightforward method for packaging the components and achieving a balanced mass distribution in the vehicle. The IMU can be designed to coincide with the vehicle's center of mass. E) Extensibility for scaling optimizations. The airframe design can be easily modified to accomodate any actuator size around this scale regime.

Additionally, the wing is attached to the transmission with a passive rotation hinge in series. The passive rotation hinge was first presented in [3] and is shown in Figure 5A. We apply the design rules outlined in [13] to increase fatigue lifetime of these hinges, but we fabricate them separately from the transmissions and wings to allow for replaceability; these hinges have previously been the first point of failure in the vehicle.

D. Airframe

For this discussion, we use the terms "airframe" to describe the vehicle's mechanical ground structure, excluding the transmission mechanism, the actuators, and the wings. The actuators are producing at least 5.1 times more force, in addition to 3 times more aerodynamics force on the wings. This increase in forces acting on the vehicle structure requires that the airframe be rigid and effective in resisting the loads with minimal structural deformation. For the actuators and the transmissions to operate effectively, they must be solidly grounded to the airframe. At the same time, other requirements stand. The airframe must be extremely lightweight. It needs to be efficiently constructed and reproduced. And the design must be extensible for electronics integration, based on known placement needs for certain electronic components.

Unlike the split actuator bee design which used a monolithic airframe, the vehicle design presented here is built in two halves. Each half consists of an airframe, actuator, transmission, and wing, and the two halves are mirror images of each other. These two halves are rigidly coupled together with carbon fiber composite beams. The hull space in between the two halves will house the electronics payload.

Some electronic components require specific orientations and placement on the vehicle structure, as described in Table I. In particular, the IMU benefits from being placed at the vehicle's center of mass to reduce translational vibration [9]. To account for a range of possible component placements, simplify the component packaging problem, and reduce structural mass, we envision placing all electronic components on a single, planar flex circuit. This flex circuit resides in the midplane of the vehicle. Knowing the vehicle structure's center of mass and the mass distribution of the populated flex circuit, we can design the flex circuit such that the IMU coincides with the center mass of the fully assembled vehicle. Figure 5D illustrates this concept.

To simultaneously resist bending loads from the bimorph actuator and torsional loads from drag forces on the wings,

the airframe halves are designed as rectangular tubes for structural efficiency. We further reduce airframe mass by using a semi-monocoque construction. The airframe is constructed from carbon fiber rigid elements and polyimide-film flexure hinges, all constructed monolithically in 2D and manually folded into a 3D structure. For the widest faces of the thin-wall beam, we extend a single membrane of polyimide film across them; the tension of this membrane reinforces the beam structure and maintains its rigidity, avoiding the added mass of a network of rigid carbon fiber struts. At this scale, the Young's modulus of the polyimide is sufficiently high to avoid stretching. To expedit construction, the airframe tubular structure is constructed via a pop-up design, as illustrated in Figure 5C. This enables the airframe to be produced very efficiently. It can also be produced with a five rigid-layer laminate, enabling the transmission to be fabricated in the same laminate batch simultaneously.

The airframe secures the actuator base with two clips that are oriented perpendicular to the plane of the actuator. This simple mounting scheme and the design of the airframe can be easily adjusted to support a range of actuator sizes (see Figure 5E), limited only by the material strength of the constituent structural features. At too large a scale, the thin composite structure will not be sufficiently rigid.

IV. Results

We were able to perform a stationary hovering flight with a 115 mg dummy payload onboard. We use the experimental setup presented in [6], which relies on an array of external motion tracking cameras (Vicon, Oxford, UK) to observe the vehicle's position and attitude in flight. This real time tracking is used with a closed-loop flight controller—presented in [7]—implemented on an offboard desktop computer and adjusted for the new vehicle's properties, to calculate appropriate control inputs (in the form of actuator signals) for specified flight behavior. Power and control signals are fed to the vehicle through a wire tether.

The robotic vehicle was able to lift off and maintain a stationary hover about a setpoint with minimal deviations in position and attitude, thus achieving the design goal of 105 mg payload capacity. The natural frequency of the flapping mechanism was experimentally determined to be 70 Hz. This is within the predicted range of the system natural frequency from Section 2A. Using a custom-built capacitive force sensor, we measured a maximum thrust force of 450 mg. The properties of the completed vehicle are summarized in Table II.

V. Discussion

The controlled flight demonstration with a 115 mg dummy payload confirms that this particular vehicle design can be control autonomous, based on the mass estimates of the required electronic components. Our measured maximum thrust force of 450 mg clearly exceeds what is required to lift and control the robotic vehicle. This thrust force measurement was performed at a high amplitude voltage signal (250V) relative to controlled flight conditions, though

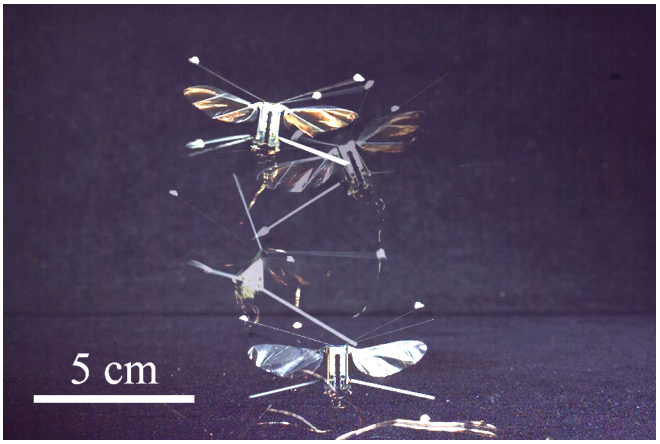

Fig. 6. Stationary hovering flight of the 265 mg robot with a 115 mg payload—380 mg total. The robot hovered 6 cm above the ground for 5 seconds. Strobed positions of the flight ascent are shown.

we chose to avoid the highest possible voltage amplitude (300V) and prevent possible damage to the vehicle prototype. We consider these optimistic results to be preliminary. More comprehesive characterization of the vehicle design is required, including stress testing for the true maximum thrust force and maximum payload capacity.

The fabrication framework used to construct the vehicles is adequately repeatable for supporting research pace. Post-assembly, we find noticeable variability, particularly in the mean wing angle of the vehicles, which is inconvenient as the flight controller gains need to be specifically tuned for individual vehicles. Though the controller can account for some of this performance variability, the corrective effort decreases the control authority margins, as described in Section 2A. Potential refinements to the fabrication process could include external mechanical fixtures and additional pop-up, auto-aligning design features to enable greater precision in the assembly of the device. The vehicle structure could also be designed with mechanisms for post-assembly, mechanical trimming.

Looking at Table II, we see that the total unloaded robot mass was greater than the scaling target, as was the actuator mass fraction. This may indicate that our actuators are oversized for the target payload capacity and could account for the resulting significant payload capacity margin. It is also possible that structural mass fraction of this scaled vehicle is more optimal than that of the split actuator bee. The thrust-to-weight ratio of the scaled vehicle was very similar to the split actuator bee; this is likely to improve with more comprehensive measurements of maximum thrust force.

Our simple scaling heuristic appears to be sufficient for predicting vehicle parameters that can result in flightworthy devices, which may indicate that the design space for flapping-wing flying vehicles at this scale is large. The heuristic emphasizes maintaining previously-verified wing kinematics. However, the underestimate in actuator and structure mass fractions suggests that the heuristic lacks fidelity, and motivates further development of a more detailed, full-

system analysis and optimization of the vehicle design.

It was beyond the scope of this work to optimize the individual system components. For future iterations, we could improve system power density by developing wings with less inertia to increase the system's natural frequency. We could also precisely characterize the expected forces acting on the airframe and optimize the airframe structural design to reduce mass and increase structural efficiency. Optimization of the actuator-transmission-wing subsystem should produce a well-matched actuator-wing pair and also increase system power density.

Nevertheless, we have developed a vehicle design that can be easily adapted for future, optimized system design parameters. At conception, this design was intended for electronics integration, and this has significantly influenced the structural design. Even with the simplistic scaling heuristic used here, we are able to obtain flightworthy results. The payload capacity as-is provides utility for the realization of control autonomy in insect-scale flying robots. We have identified a promising, scalable vehicle design and fabrication framework that, in tandem with more-developed modeling and optimization of system, will leave the integration of an onboard power source as the last major research hurdle toward control and power autonomous operation of robotic flying insects. Candidate technologies for the power source include micro fuel cells [23], solar cells, conventional-, and novel-structured lithium ion batteries [24].

ACKNOWLEDGMENTS

The authors thank Farrell Helbling for assisting with the controlled flight experiments and for fruitful discussions.

REFERENCES

[1] M. Keennon, K. Klingebiel, H. Won, and A. Andriukov, "Development of the nano hummingbird: A tailless flapping wing micro air vehicle," in *AIAA Aerospace Sciences Meeting*, 2012, pp. 1–24.

[2] D. Lentink, S. R. Jongerius, and N. L. Bradshaw, "The scalable design of flapping micro-air vehicles inspired by insect flight," in *Flying insects and robots*. Springer, 2010, pp. 185–205.

[3] R. J. Wood, "The first takeoff of a biologically inspired at-scale robotic insect," *Robotics, IEEE Transactions on*, vol. 24, no. 2, pp. 341–347, 2008.

[4] P. S. Sreetharan, J. P. Whitney, M. D. Strauss, and R. J. Wood, "Monolithic fabrication of millimeter-scale machines," *Journal of Micromechanics and Microengineering*, vol. 22, no. 5, p. 055027, 2012.

[5] K. Y. Ma, S. M. Felton, and R. J. Wood, "Design, fabrication, and modeling of the split actuator microrobotic bee," in *Intelligent Robots and Systems (IROS), 2012 IEEE/RSJ International Conference on*. IEEE, 2012, pp. 1133–1140.

[6] K. Y. Ma, P. Chirarattananon, S. B. Fuller, and R. J. Wood, "Controlled flight of a biologically inspired, insect-scale robot," *Science*, vol. 340, no. 6132, pp. 603–607, 2013.

[7] P. Chirarattananon, K. Y. Ma, and R. J. Wood, "Single-loop control and trajectory following of a flapping-wing microrobot," in *Robotics and Automation (ICRA), 2014 IEEE International Conference on*. IEEE, 2014, pp. 37–44.

[8] S. B. Fuller, M. Karpelson, A. Censi, K. Y. Ma, and R. J. Wood, "Controlling free flight of a robotic fly using an onboard vision sensor inspired by insect ocelli," *Journal of The Royal Society Interface*, vol. 11, no. 97, p. 20140281, 2014.

[9] S. B. Fuller, E. F. Helbling, P. Chirarattananon, and R. J. Wood, "Using a MEMS gyroscope to stabilize the attitude of a fly-sized hovering robot," in *IMAV 2014: International Micro Air Vehicle Conference and Competition 2014, Delft, The Netherlands, August 12-15, 2014*. Delft University of Technology, 2014.

[10] E. F. Helbling, S. B. Fuller, and R. J. Wood, "Pitch and yaw control of a robotic insect using an onboard magnetometer," in *Robotics and Automation (ICRA), 2014 IEEE International Conference on*. IEEE, 2014, pp. 5516–5522.

[11] C. P. Ellington, "The novel aerodynamics of insect flight: applications to micro-air vehicles," *Journal of Experimental Biology*, vol. 202, no. 23, pp. 3439–3448, 1999.

[12] J. Whitney and R. Wood, "Conceptual design of flapping-wing micro air vehicles," *Bioinspiration & biomimetics*, vol. 7, no. 3, p. 036001, 2012.

[13] R. Malka, A. L. Desbiens, Y. Chen, and R. J. Wood, "Principles of microscale flexure hinge design for enhanced endurance," in *Intelligent Robots and Systems (IROS 2014), 2014 IEEE/RSJ International Conference on*. IEEE, 2014, pp. 2879–2885.

[14] N. T. Jafferis, M. J. Smith, and R. J. Wood, "Design and manufacturing rules for maximizing the performance of polycrystalline piezoelectric bending actuators," *Smart Materials and Structures*, 2015.

[15] X. Zhang, T. Tong, D. Brooks, and G.-Y. Wei, "Evaluating adaptive clocking for supply-noise resilience in battery-powered aerial microrobotic system-on-chip," 2014.

[16] M. Karpelson, G.-Y. Wei, and R. J. Wood, "Milligram-scale high-voltage power electronics for piezoelectric microrobots," in *Robotics and Automation, 2009. ICRA'09. IEEE International Conference on*. IEEE, 2009, pp. 2217–2224.

[17] P.-E. Duhamel, N. O. Perez-Arancibia, G. L. Barrows, and R. J. Wood, "Biologically inspired optical-flow sensing for altitude control of flapping-wing microrobots," *Mechatronics, IEEE/ASME Transactions on*, vol. 18, no. 2, pp. 556–568, 2013.

[18] B. M. Finio, N. O. Pérez-Arancibia, and R. J. Wood, "System identification and linear time-invariant modeling of an insect-sized flapping-wing micro air vehicle," in *Intelligent Robots and Systems (IROS), 2011 IEEE/RSJ International Conference on*. IEEE, 2011, pp. 1107–1114.

[19] A. J. Bergou, S. Xu, and Z. Wang, "Passive wing pitch reversal in insect flight," *Journal of Fluid Mechanics*, vol. 591, pp. 321–337, 2007.

[20] A. L. Desbiens, Y. Chen, and R. J. Wood, "A wing characterization method for flapping-wing robotic insects," in *Intelligent Robots and Systems (IROS), 2013 IEEE/RSJ International Conference on*. IEEE, 2013, pp. 1367–1373.

[21] J. H. Marden, "Maximum lift production during takeoff in flying animals," *Journal of Experimental Biology*, vol. 130, no. 1, pp. 235–258, 1987.

[22] R. Wood, E. Steltz, and R. Fearing, "Optimal energy density piezoelectric bending actuators," *Sensors and Actuators A: Physical*, vol. 119, no. 2, pp. 476–488, 2005.

[23] A. Evans, A. Bieberle-Hütter, J. L. Rupp, and L. J. Gauckler, "Review on microfabricated micro-solid oxide fuel cell membranes," *Journal of Power Sources*, vol. 194, no. 1, pp. 119–129, 2009.

[24] K. Sun, T.-S. Wei, B. Y. Ahn, J. Y. Seo, S. J. Dillon, and J. A. Lewis, "3D printing of interdigitated Li-Ion microbattery architectures," *Advanced Materials*, vol. 25, no. 33, pp. 4539–4543, 2013.